

3-D Position Optimization of Solar-Powered Hovering UAV Relay in Optical Wireless Backhaul

Heyou Liu, Muhammad Salman Bashir, *Senior Member, IEEE*, Mohamed-Slim Alouini, *Fellow, IEEE*

Abstract—A major hurdle in widespread deployment of UAVs (unmanned aerial vehicle) in existing communications infrastructure is the limited UAV onboard energy. Therefore, this study considers solar energy harvesting UAVs for wireless communications. In this context, we consider three dimensional position optimization of a solar-powered UAV relay that connects a distant sensor field to an optical ground station (OGS) for data processing. The integrated sensor-UAV-OGS network utilizes radio frequency band for sensor-to-UAV links and the optical band for the UAV-to-OGS feeder link. Since atmospheric conditions affect both the harvested solar energy as well as the optical wireless signal, this study tackles UAV position optimization problems under various channel conditions such as clouds, atmospheric turbulence and dirt. From this study, we discover that the optimum position of the UAV—that maximizes the end-to-end channel capacity—is heavily dependent on the atmospheric channel conditions.

Index Terms—Channel capacity, cloud, optical wireless signal, position optimization, solar energy harvesting relay, unmanned aerial vehicle.

I. INTRODUCTION

Unmanned Aerial Vehicles (UAVs) are revolutionizing traditional paradigms in contemporary wireless communication. Their unique ability to navigate difficult terrains and regions grants UAVs a substantial advantage in terms of deployment flexibility, cost efficiency, and adaptability over static relaying methods [1], [2]. This is particularly advantageous in areas without ground infrastructure or where ground terminals are separated by obstacles such as mountains or buildings as UAVs can essentially provide line-of-sight (LoS) connectivity and enhanced capacity [3], [4]. The mobility of UAVs is ideal for on-demand operations and can significantly improve communication channels, primarily through the establishment of short-distance LoS links [5], [6]. Utilized as aerial base stations, UAVs are particularly beneficial in scenarios that demand immediate and adaptable wireless service, such as in temporary hotspots and emergency situations. The enhanced availability of LoS connections due to UAVs' elevated positions, combined with their high maneuverability, allows for a fast and highly flexible deployment of communication infrastructure in time-sensitive or economically restrictive environments [7], [8].

A. Problem Motivation

Despite their extensive applications, the deployment of UAVs in communication systems encounters significant chal-

lenges, predominantly related to onboard energy storage limitations. The UAVs' endurance and performance are directly restricted by the finite energy reserves due to size and weight constraints of aerial platforms [9]–[11]. This necessitates a strategic focus on energy-efficient communications and exploitation of energy harvesting techniques to maximize the operational time of the UAV. Two popular energy harvesting techniques for optical wireless based UAVs are i) *simultaneous lightwave information and power transfer* (SLIPT) in which the data carrying laser beam from the ground is also used to power the UAV [12]–[14] and ii) solar-powered UAVs that harvest sunlight energy to either partially or fully meet their power requirements [8], [15], [16].

There are only a few studies that discuss the trajectory/position optimization of solar-powered UAVs to maximize some quality-of-service metric (such as channel capacity) in wireless communications. Specifically, articles [8], [17] thoroughly discuss the resource allocation and trajectory optimization of a solar-powered UAV to maximize the sum rate in the multi-user and multi-sensor links, respectively. Both these studies consider RF channels to communicate with users/sensors. However, for serial RF/FSO links in which the UAV connects the multi-user (or multi-sensor) side to an optical ground station (OGS) through i) RF (user-to-UAV) links and ii) a feeder FSO (UAV-to-OGS) link, position optimization of a UAV relay incurs extra considerations which have not been addressed before to the best of our understanding. Firstly, for the two-dimensional UAV position optimization (for UAVs obtaining sufficient sunlight even at lower heights), the end-to-end rate is limited not only by the user-to-UAV RF link but also the UAV-to-OGS optical link. Secondly, for UAVs limited by solar energy, atmospheric effects—such as clouds and dirt—will play a major role not only in affecting the harvested solar energy but also the FSO laser signal connecting the UAV and the OGS. Thirdly, for the solar energy limited UAV, UAV position optimization incurs certain tradeoffs between maximizing harvested solar energy and the end-to-end rate of the serial RF/FSO link. All these considerations form the motivation of the current study which deals with the optimization of a solar-powered UAV relay position in an RF/FSO communication system.

B. Background Literature Review

Recent literature on energy efficient UAV-based wireless communication systems considers research efforts primarily focused on two interrelated objectives: energy resources optimization and UAV placement (or UAV trajectory) strategies

H. Liu and M.-S. Alouini are with the CEMSE Division, King Abdullah University of Science and Technology (KAUST), Thuwal 23955-6900, Kingdom of Saudi Arabia. M. S. Bashir is with the School of Computing and Engineering, University of Huddersfield, Huddersfield HD1 3DH United Kingdom. e-mail: (heyou.liu@kaust.edu.sa; m.bashir@hud.ac.uk; slim.alouini@kaust.edu.sa)

to enhance system performance. A core aspect involves the UAVs' role as either aerial base stations, or relays, to enhance support for ground users [18]. Trajectory optimization emerges as a key question in the study [19] which optimizes UAV relay paths to maximize ground terminal throughput and improve static relaying methods. In [6], trajectory optimization also accounts for energy efficiency by considering propulsion energy consumption alongside communication throughput. Articles [2], [20] collectively examine joint optimization of transmission power, bandwidth, and UAV positioning to improve the overall performance of UAV-assisted networks. The works [21], [22] discuss power consumption concerns which focus on minimizing uplink power for ground users and exploring energy-constrained operational strategies, respectively.

Limited onboard energy has forced the UAV design in recent years to focus on an energy-efficient paradigm. To address the finite battery life, which is a critical limitation for UAVs, some studies such as [1], [2], [7], [23] have proposed comprehensive energy consumption models that take into account various aspects and functions of UAVs. However, reliance on onboard batteries for UAV-based communication systems leads to limited operation times. The frequent need for these UAVs to return to base for recharging hinders the stability and sustainability of communication services, thus creating system performance bottlenecks. Although direct battery replacement or recharging is a straightforward approach to extend operational life, it becomes impractical and labor-intensive when scaling up to a large number of UAVs or sensors [22]. Thus, seeking innovative methods to bolster the energy framework of UAVs to support extended and reliable operations continues to be a critical challenge in the design and deployment of UAV communication systems.

To overcome the limitations of conventional battery systems due to finite on-board energy, the potential of solar-powered UAVs has been explored in recent literature. The authors in [15], [16] described the development of solar-powered UAV prototypes that leverage solar panels to efficiently convert solar energy into electrical power to enable extended flight duration. The authors in [24] introduce the idea and implementation of solar-powered UAVs as base stations for 5G and beyond systems. The concept of solar-powered UAVs is further exemplified by prototypes that have successfully demonstrated long-endurance flights exceeding a full day [8], [11]. This technology has garnered interest for its implications in both military and civilian spheres, particularly for tasks requiring prolonged aerial presence such as reconnaissance and surveillance [25]. The advancement in solar cell materials technology, specifically the use of flexible and lightweight cells, is pivotal for the integration of solar energy into UAV systems. The authors in [26] explored solar cells materials characterized by their nanocrystalline structure, robust light absorption across a wide spectrum and suitability for deployment on flexible substrates. These materials are pivotal for crafting ultra-lightweight and adaptable solar cells that can be seamlessly integrated into UAV designs to enhance their operational efficiency and expanding their utility in both aerial and terrestrial domains. Furthermore, the exploration of solar power extends beyond UAVs to other realms of transportation

such as the six-seat transporter flight referenced in [27]. These innovations in solar cell materials and construction techniques have enhanced the practicality of solar-powered UAVs and broaden their application spectrum.

This work is motivated by the idea that the efficacy of solar energy harvesting in UAV applications is closely intertwined with the UAV's operational altitude, as discussed in [8], [25], [28]. Atmospheric transmittance, a critical determinant of the solar energy captured by UAV-mounted photovoltaic cells, diminishes at lower altitudes due to increased air density and potential obstructions such as clouds. This attenuation of solar irradiance at reduced altitudes consequently affects the solar energy flux available for conversion to electrical power. Conversely, as UAVs ascend to higher altitudes, they benefit from increased atmospheric transmittance, thereby enhancing the solar energy harvest. Yet, this advantage is not without its trade-offs. Elevated altitudes, while favorable for solar energy collection, concurrently escalate the path loss in air-to-ground communication links, presenting a trade-off that necessitates a balanced approach to optimize both solar energy harvesting and communications performance [8], [17]. Therefore, the design of UAV systems requires a careful consideration of these conflicting aspects to ensure an optimal balance between energy harvesting and communication quality. In addition, the authors in [7] and [18] investigated the strategic 3-D deployment of UAVs, targeting optimal user coverage and service area expansion, with the former focusing on maximizing network revenue, and the latter on the deployment of UAVs as aerial base stations with directional antennas. Besides, the optimization of solar energy capture through intelligent path design is detailed in [29] which employs quaternion-based methods, whereas the work in [25] improves solar-powered UAV endurance by optimizing flight paths to exploit gravitational potential and attitude adjustments. The joint optimization of 3-D positioning trajectory and resource allocation is analyzed in studies [7], [30], to enhance system throughput and extend UAV flight endurance. Expanding on these endeavors, the authors in [31] and [32] presented energy-efficient trajectory schemes that merge solar energy harvesting with charging stations, thereby constructing a sustainable communication service framework for UAV-assisted networks. The comprehensive approach in [8] incorporates trajectory planning with resource allocation for multi-carrier systems to maximize operational efficiency over extended periods. Moreover, the authors in [33] developed a greedy algorithm augmented with a buffering mechanism to compute optimal flight trajectories that enables perpetual flight in solar-powered aircraft. In a similar vein, the work [34] presented a mission-oriented design approach for three-dimensional (3D) path planning of solar-powered unmanned aerial vehicles. This approach strategically utilizes limited solar energy resources to optimize the effectiveness of the mission. The article [22] explored a solar-powered UAV that is tasked with data collection from Internet of Things Devices (IoTds) and providing energy to them through laser. The main focus of this article is on maximizing the UAV's residual energy by jointly optimizing the IoTds' scheduling and the UAV's three-dimensional trajectory. An innovative iterative algorithm—that integrates

block coordinate descent and successive convex optimization techniques—is recommended to efficiently address the simultaneous optimization of user scheduling and UAV path planning.

Overall, these references underscore the critical goal of achieving optimal UAV performance through a focus on solar power utilization and 3-D positioning. Thus, it is essential to formulate an integrated optimization strategy that encapsulates both altitude-dependent solar energy harvesting and the end-to-end performance of communication system under different environment conditions. This strategy should account for the UAV’s flight trajectory or position, thereby ensuring optimal energy efficiency, maximum data transmission rates, and reliable communication.

C. Contributions of Current Study

The main contributions of this paper can be summarized as follows:

- 1) The first contribution is the derivation of (approximate) closed-form solutions for optimal UAV position in two dimensions for the aggregate sensor-to-UAV channel (Section III). These approximate solutions are highly accurate in asymptotic regimes. Furthermore, for the aggregate channel, we present a novel closed-form solution to determine the UAV’s optimal coordinates within a max-min fairness framework.
- 2) For the end-to-end link, the role of a solar-powered UAV as an amplify-and-forward (AF) and decode-and-forward (DF) relay is explored (Section V). A number of asymptotic scenarios were covered for such relays which gave us deeper insights and helped us explain the optimization results pertaining to the optimum altitude of a solar-powered UAV relay.
- 3) For the end-to-end link that comprises sensor-to-UAV and UAV-to-OGS links, we assessed the impacts of atmospheric turbulence and cloud layers on laser signal attenuation as well as the harvested solar energy, and explored their influence on the UAV’s optimal positioning (Section VI). The criterion for optimal UAV positioning is the end-to-end channel capacity that is maximized for the UAV’s role as both an amplify-and-forward (AF) and decode-and-forward (DF) relay. Various insights for optimal 2-D and 3-D positioning of UAV relay—based on atmospheric conditions—are developed.

D. Model Assumptions

To simplify the analysis, we now consider the following two major assumptions (along with justifications) in our study.

- 1) We assume that the uplink RF channel between each sensor and the UAV is dominated by the LoS component. This assumption holds well since the beamwidth (in meters) from the transmitting sensor is small close to the ground and most sensors are “looking upwards” to the UAV while transmitting. This arrangement implies that the reflections from the ground objects are at a minimum, and therefore, the assumption of the dominance

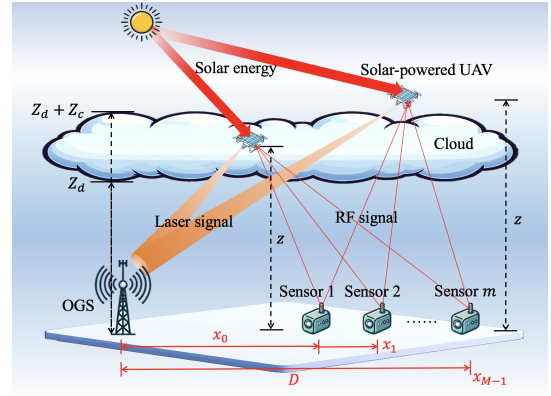


Fig. 1. This figure depicts the system model of a UAV-assisted serial RF/FSO link. This figure shows two scenarios where, in the first scenario, the UAV lies inside the cloud, and in the other scenario, the UAV hovers on top of the clouds.

of LoS holds. Additionally, for the sake of simplicity, we assume that the RF signal experiences nominal fading in the LoS channel.

- 2) The optical wireless feeder link from the UAV-to-OGS is modeled by the (signal independent) Gaussian noise at the OGS receiver. This assumption holds under moderate signal strength conditions at the OGS receiver. Here, we have used the assumption that the received signal is neither too large so that the signal-dependent shot noise model applies, nor the signal strength is so weak that the Poisson model is justified.

E. Paper Organization

This paper is organized as follows. Section II presents the composite optical channel model in the UAV-to-OGS backhaul link. This is followed by Section III that considers two-dimensional position optimization (in the (x, y) plane) of a UAV relay for the RF based aggregate sensor-to-UAV link. The results obtained in this section give important insights for maximization of end-to-end rate of the serial RF/FSO link. Section IV focuses on solar energy harvesting and energy consumption models of a hovering UAV. The results obtained in both Section III and Section IV are utilized in maximization of end-to-end rate in Section V. The three-dimensional position optimization of a solar-powered UAV relay, along with a commentary on experimental results, is analyzed in Section VI. The main results of this study are summarized and concluded in Section VII.

II. BACKHAUL OPTICAL SIGNAL FADING MODELS

The (composite) channel gain of the UAV-OGS optical wireless link is given by

$$\mathfrak{h} = \mathfrak{h}_p \mathfrak{h}_s h_c h_a, \quad (1)$$

where \mathfrak{h}_p represents the loss in energy due to pointing error and \mathfrak{h}_s corresponds to signal fading due to scintillation of the optical signal caused by atmospheric turbulence. The deterministic coefficients, h_c and h_a , denote the attenuation of the backhaul channel due to (scattering and absorption) through cloud and air, respectively.

A. Pointing Error Model

For a circularly symmetric Gaussian pointing error distribution in two dimensions, the magnitude of the error, R , is distributed as a Rayleigh random variable. In this case, the random channel coefficient is [35]

$$\mathbb{h}_p \approx \frac{a_d^2}{2\theta^2(x^2 + y^2 + z^2)} \exp\left(-\frac{R^2}{2\theta^2(x^2 + y^2 + z^2)}\right), \quad (2)$$

and the distribution of \mathbb{h}_p is [14]

$$f_{\mathbb{h}_p}(h) = \Phi h^{(\theta^2 - \sigma^2)/\sigma^2} \cdot \mathbb{1}_{[0, B)}(h), \quad (3)$$

where θ and σ are the angular beamwidth and angular pointing error standard deviation, respectively. Assuming that the OGS lies at the origin $(0, 0, 0)$, the point (x, y, z) represents the location coordinate of the UAV relay, $\mathbb{1}_A$ is the indicator function over a measurable set A , and

$$\Phi := \frac{\theta^2}{\sigma^2} \left(\frac{1}{B}\right)^{\theta^2/\sigma^2}, \quad (4)$$

$$B := \frac{a_d^2}{2\theta^2(x^2 + y^2 + z^2)}. \quad (5)$$

The factor a_d in (5) is the radius of OGS receiver telescope.

B. Atmospheric Attenuation for Cloud and Air Model

We assume that the cloud layer is parallel to the ground and that both the upper and lower boundaries of the cloud layer remain parallel to each other (as shown in Fig. 1). Then, by the principles of similar triangles, we can deduce the link distance, d_c , through the cloud as

$$\begin{aligned} \frac{Z_c}{z} &= \frac{d_c}{\sqrt{x^2 + y^2 + z^2}}, \quad z > Z_c + Z_d \\ \frac{z - Z_d}{z} &= \frac{d_c}{\sqrt{x^2 + y^2 + z^2}}, \quad Z_d < z < Z_c + Z_d \\ \Rightarrow d_c &= \begin{cases} \frac{Z_c}{z} \sqrt{x^2 + y^2 + z^2}, & z > Z_c + Z_d \\ \frac{z - Z_d}{z} \sqrt{x^2 + y^2 + z^2}, & Z_d < z < Z_c + Z_d \\ 0, & z < Z_d, \end{cases} \end{aligned} \quad (6)$$

where Z_c is the thickness of cloud and Z_d is the distance from the ground to the lower cloud boundary. Thus, the link distance during the air is $d_a = \sqrt{x^2 + y^2 + z^2} - d_c$. Then, the values of channel coefficients, \mathbb{h}_c and \mathbb{h}_a , are given by

$$\mathbb{h}_c := e^{-\psi_c d_c}, \quad (7)$$

$$\mathbb{h}_a := e^{-\psi_a d_a}, \quad (8)$$

where ψ_c and ψ_a are the extinction coefficients that determine the attenuation of the signal (due to scattering or absorption) in the cloud and air, respectively.

C. Scintillation Due to Atmospheric Turbulence

The exponentiated Weibull distribution has been shown to provide an excellent fit to experimental results for both weak and moderate turbulence conditions compared to lognormal and Gamma-Gamma distributions [36]. An attractive feature of exponentiated Weibull distribution is the mathematically

tractable nature of its probability density function, which is given by the expression

$$f_{\mathbb{h}_s}(h) = \frac{ab}{\eta} \left(\frac{h}{\eta}\right)^{b-1} \exp\left(-\left(\frac{h}{\eta}\right)^b\right) \left(1 - \exp\left(-\left(\frac{h}{\eta}\right)^b\right)\right)^{a-1}, \quad h > 0. \quad (9)$$

In (9), b is the shape parameter which is representative of the scintillation index. The factor a is also a shape parameter that depends on receiver aperture size, and η is the scale parameter.

D. Overall Channel Model

The overall channel gain—based on channel impairments in (3), (7), (8) and (9)—is the product of individual channel impairments: $\mathbb{h} = \mathbb{h}_p \mathbb{h}_s \mathbb{h}_a \mathbb{h}_c$. Then, the overall channel probability density function is

$$f_{\mathbb{h}}(h) = \int_0^{h_a h_c B} \frac{1}{h_a h_c x} f_{\mathbb{h}_p}\left(\frac{x}{h_a h_c}\right) f_{\mathbb{h}_s}\left(\frac{h}{x}\right) dx, \quad h > 0. \quad (10)$$

III. TWO-DIMENSIONAL POSITION OPTIMIZATION OF UAV FOR SENSOR-TO-UAV LINK

We first introduce the UAV location optimization as a two-dimensional problem in which we optimize the (x, y) coordinates of UAV location to maximize the sum rate from the ground sensors. We assume that the height z of the UAV from the ground is fixed. This implies that (x, y, z) is the three dimensional position of the UAV. Two dimensional location optimization holds for scenarios when the UAV does not need solar energy to sustain itself in the air, and the UAV is suspended at the smallest possible height from the ground to establish a clear line-of-sight (LoS) with the OGS. The results obtained in this section will be utilized in later sections where we optimize the position of an energy constrained, solar-powered UAV relay.

Let us assume that the uplink radio channel between each sensor and the UAV is dominated by the LoS component. Under the Gaussian channel assumption, the maximum achievable rate (in nats/s/Hz) in the m th uplink channel—between the m th sensor and the UAV—is $C_m = \ln\left(1 + \frac{P_m G_m}{\sigma_0^2}\right)$, where P_m is the power transmitted by the m th sensor, and G_m is the power gain of the channel for the case when the line-of-sight dominates other paths between the sensor and the UAV [12]. The parameter σ_0^2 represents the thermal noise power at the UAV antenna. The quantity G_m is defined as

$$G_m := \frac{\beta_0}{z^2 + (x_m - x)^2 + (y_m - y)^2}, \quad (11)$$

where z is the height of the UAV from ground in meters, (x_m, y_m) is the location of the m th sensor on ground and $\sqrt{(x_m - x)^2 + (y_m - y)^2}$ is the distance of the m th sensor from the UAV. The quantity β_0 represents the channel power gain at the reference distance of 1 meters from the sensor. The sum rate in the aggregate sensor channel, denoted by C_s , is $C_s := \sum_{m=0}^{M-1} C_m$, where M is the total number of sensors

deployed in the region. Let us assume that the m th sensor is located at position x_m for $0 \leq m \leq M-1$. We then have that

$$C_s = \sum_{m=0}^{M-1} \ln \left(1 + \frac{P_m \beta_0}{\sigma_0^2 [z^2 + (x - x_m)^2 + (y - y_m)^2]} \right). \quad (12)$$

A. Optimization Problem 1

$$\begin{aligned} & \underset{x,y}{\text{maximize}} && C_s \\ & \text{subject to} && x > 0, y > 0. \end{aligned} \quad (13)$$

1) *SNR reasonably large*: Let us assume that P_m is large enough so that the SNR in the m th sensor channel, denoted by λ_m , is

$$\lambda_m := \frac{P_m \beta_0}{\sigma_0^2 [z^2 + (x - x_m)^2 + (y - y_m)^2]} > 1 \quad (14)$$

for all m . The approximation

$$\ln(1 + \lambda_m) \approx \gamma \left((1 + \lambda_m)^{\frac{1}{\gamma}} - 1 \right), \quad (15)$$

holds for a large enough number γ [14]. Equation (15) can be rewritten as $\ln(1 + \lambda_m) \approx \gamma \left(\lambda_m^{\frac{1}{\gamma}} \left(1 + \frac{1}{\lambda_m} \right)^{\frac{1}{\gamma}} - 1 \right)$. Since $\frac{1}{\lambda_m} < 1$ and $\frac{1}{\gamma} \frac{1}{\lambda_m} \ll 1$, we can use binomial theorem to approximate $\left(1 + \frac{1}{\lambda_m} \right)^{\frac{1}{\gamma}} \approx 1 + \frac{1}{\gamma \lambda_m}$. Thus,

$$\ln(1 + \lambda_m) \approx \gamma \left(\lambda_m^{\frac{1}{\gamma}} \left(1 + \frac{1}{\gamma \lambda_m} \right) - 1 \right) = \gamma \lambda_m^{\frac{1}{\gamma}} + \lambda_m^{\frac{1}{\gamma}-1} - \gamma. \quad (16)$$

Substituting approximation (16) into (12), we have that the final expression for C_s (for reasonably large SNR) is

$$C_s \approx \sum_{m=0}^{M-1} \left(\gamma \lambda_m^{\frac{1}{\gamma}} + \lambda_m^{\frac{1}{\gamma}-1} - \gamma \right). \quad (17)$$

Now, taking the partial derivatives of C_s (Equation (17)) with respect to x and y and setting the derivatives equal to 0, we have that

$$\begin{aligned} \frac{\partial}{\partial x} C_s &= \sum_{m=0}^{M-1} \frac{\sigma_0^2}{P_m \beta_0} (x - x_m) \\ & - \sum_{m=0}^{M-1} \frac{1}{(z^2 + (x - x_m)^2 + (y - y_m)^2)} (x - x_m) = 0, \end{aligned} \quad (18)$$

$$\begin{aligned} \frac{\partial}{\partial y} C_s &= \sum_{m=0}^{M-1} \frac{\sigma_0^2}{P_m \beta_0} (y - y_m) \\ & - \sum_{m=0}^{M-1} \frac{1}{(z^2 + (x - x_m)^2 + (y - y_m)^2)} (y - y_m) = 0. \end{aligned} \quad (19)$$

When z is large enough so that $z^2 \gg (x - x_m)^2 + (y - y_m)^2$ for all m , then a solution to (18) and (19) is obtained as

$$x^* = \frac{\sum_{m=0}^{M-1} x_m \left(\frac{\sigma_0^2}{P_m \beta_0} - \frac{1}{z^2} \right)}{\sum_{m=0}^{M-1} \left(\frac{\sigma_0^2}{P_m \beta_0} - \frac{1}{z^2} \right)}, \quad (20)$$

$$y^* = \frac{\sum_{m=0}^{M-1} y_m \left(\frac{\sigma_0^2}{P_m \beta_0} - \frac{1}{z^2} \right)}{\sum_{m=0}^{M-1} \left(\frac{\sigma_0^2}{P_m \beta_0} - \frac{1}{z^2} \right)}. \quad (21)$$

2) *Low SNR scenario*: When $\lambda_m \ll 1$, we have that $\ln(1 + \lambda_m) \approx \lambda_m$ and $C_s \approx \sum_{m=0}^{M-1} \lambda_m$. In this case, it can be shown that for $z^2 \gg (x - x_m)^2$ for all m , the optimal value of x is

$$x^* \approx \frac{\sum_{m=0}^{M-1} P_m x_m}{\sum_{m=0}^{M-1} P_m}, \quad (22)$$

$$y^* \approx \frac{\sum_{m=0}^{M-1} P_m y_m}{\sum_{m=0}^{M-1} P_m}. \quad (23)$$

3) *Approximation Error Plots*: Here, we consider the error in approximate solutions (20) (21), (22) and (23) to the optimization problem (13). Let the exact (numerical) solution to (13) be denoted by (\tilde{x}, \tilde{y}) . We then use the normalized mean-square error to quantify the approximation error:

$$\text{NMSE} = \frac{(x^* - \tilde{x})^2 + (y^* - \tilde{y})^2}{\tilde{x}^2 + \tilde{y}^2}, \quad (24)$$

where (x^*, y^*) are the analytical (approximate) solutions furnished by (20) and (21) for large SNR; and (22) and (23) for low SNR. Fig. 2 illustrates the NMSE for low SNR (left figure) and high SNR (right figure) approximations for varying channel power gains at the reference distance β_0 and at different UAV altitudes represented by z . It is noteworthy that the approximate expressions maintain a high level of accuracy both at low ($\lambda_m \ll 1$) and high SNR regimes ($\lambda_m \gg 1$), particularly within the regions demarcated by dashed regions. However, for the low SNR scenario, the approximation tends to diminish in accuracy as the SNR elevates, especially for $\sigma_0^2 < 10^{-5}$. Similarly, for the high SNR scenario, the approximation error begins to grow for $\sigma_0^2 > 10^{-9}$. We also note that the variation in β_0 seems to have a nominal effect on the NMSE for both SNR extremities. Yet, a declining UAV altitude begins to erode the approximations' precision since the approximate solutions were computed based on the assumption $z^2 \gg (x - x_m)^2 + (y - y_m)^2$. For the said figure, the location of sensors are $\mathbf{x}_m = [0, 100, 150, 200, 250, 350, 450, 550, 750, 1000]$, $\mathbf{y}_m = [0, 150, 250, 300, 450, 550, 650, 700, 800, 1000]$, the power transmitted by the sensor is $\mathbf{P}_m = [0.5, 1.0, 1.5, 2.0, 2.5, 3.0, 3.5, 4.0, 4.5, 5.0]$.

Fig. 3 presents the aggregate sensor channel capacity C_s contingent upon the UAV's spatial positioning. This emphasizes the significance of strategic UAV placement to enhance channel performance. For this figure, the default system parameters are the same as Fig. 2.

B. Optimization Problem 2

$$\begin{aligned} & \underset{x,y}{\text{maximize}} && \min_m C_m \\ & \text{subject to} && x \geq x_0, y \geq y_0. \end{aligned} \quad (25)$$

A closed-form solution results for the above mentioned problem results when the sensors are arranged in a nondecreasing power sequence from left to right. This arrangement

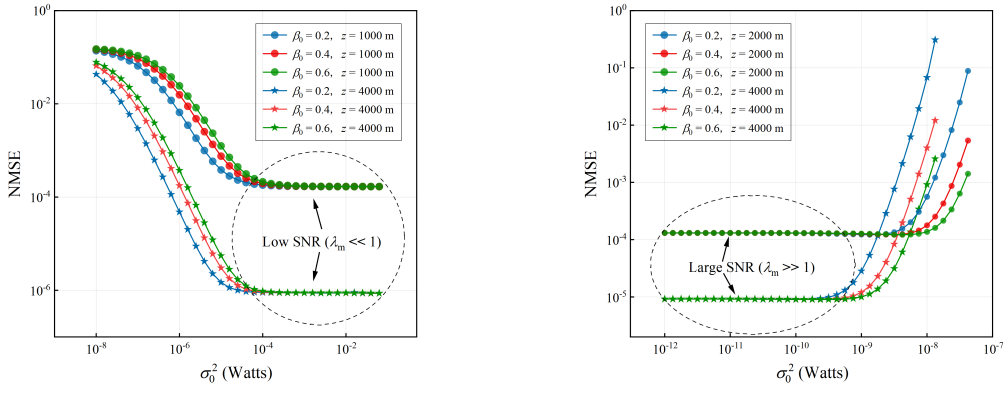


Fig. 2. This figure shows the normalized mean-square error as a function of σ_0^2 for low (left) and large (right) SNR scenarios with different values of factor β_0 and the height of UAVs z . The total link distance $D = 1000$ m, the number of the sensors is $M = 10$ and the height of UAV $z = 5000$ m.

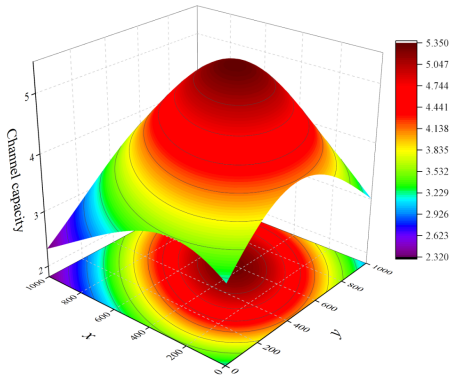


Fig. 3. The figure shows 3-D plot of the aggregate sensor-to-UAV channel capacity as a function of UAV's location in two dimensions. The UAV height $z = 500$ m and $\beta_0 = 0.4$. The noise power $\sigma_0^2 = 1 \times 10^{-6}$ W.

implies that $P_0 \leq P_1 \leq \dots \leq P_{M-1}$. This is a natural arrangement in that we place the lower power sensors closer to the OGS and the larger power sensors further away. For a better understanding of problem (25), we will first consider the solution to one-dimensional problem in terms of x (by fixing the value of y) and then extend the solution to the two-dimensional problem for (x, y) . The one-dimensional analog of (25) is

$$\begin{aligned} & \underset{x}{\text{maximize}} && \min_m C_m \\ & \text{subject to} && x \geq x_0. \end{aligned} \quad (26)$$

1) *Solution of One-Dimensional Problem:* For the one-dimensional optimization problem, we fix the value of y and maximize capacity as a function of only x coordinates. For the sake of brevity, we represent the uplink capacity of the m th sensor, $C_m(x, y)$, as $C_m(x)$ to highlight the one-dimensional nature of the problem.

For the one-dimensional problem, the solution is given by the following two-step algorithm:

- 1) For a fixed value of y , find the set \mathcal{X} of non-negative UAV positions: $\mathcal{X} := \{x^{(1)}, x^{(2)}, \dots, x^{(M-1)}\}$, such that

$$C_0(x^{(i)}) = C_i(x^{(i)}), \quad (27)$$

for $i = 1, 2, \dots, M - 1$.

- 2) The solution of optimization problem (26) is $x^* = \max \mathcal{X}$. The maximized value of minimum capacity is $C^* = C_0(x^*)$.

a) *Proof:* For the nondecreasing power arrangement, let us define the sequence of M points $x^{(i)} > 0$, for $i = 0, 1, 2, \dots, M - 1$. The point $x^{(i)}$ is defined as the position of the UAV relay where the capacity C_i is equal to C_0 (or the point where the two capacity curves, C_i and C_0 , intersect):

$$\begin{aligned} C_i(x^{(i)}) = C_0(x^{(i)}) & \implies \frac{P_i}{z^2 + (x^{(i)} - x_i)^2} = \frac{P_0}{z^2 + (x^{(i)} - x_0)^2} \\ & \implies (x^{(i)})^2 (P_i - P_0) + x^{(i)} (2P_0x_i - 2P_ix_0) \\ & \quad + P_ix_0^2 - P_0x_i^2 + (P_i - P_0)z^2 = 0. \end{aligned} \quad (28)$$

The equation (28) is a quadratic in $x^{(i)}$ and can be solved by using the well-known quadratic formula: $x^{(i)} = \frac{-b + \sqrt{b^2 - 4ac}}{2a}$, where $a := P_i - P_0$, $b := 2(P_0x_i - P_ix_0)$ and $c := P_ix_0^2 - P_0x_i^2 + (P_i - P_0)z^2$.

Before we move further, we need to address an important point. Since the curve C_0 corresponds to the smallest power, it will determine the minimum rate beyond a certain point \hat{x} , where $\hat{x} > x_{M-1}$. For some $x > \hat{x}$, $\min_m C_m(x) = C_0(x)$ since $P_0 < P_m$ and $|x_0 - x| > |x_m - x|$ for any $m > 0$. In this case, $C_0(x)$ is a monotonically decreasing function in x for $x > \hat{x}$.

However, if x approaches $-\infty$ from the point \hat{x} , $C_0(x)$ —and therefore $\min(C_m)$ —will increase and intersect some $C_j(x)$, $j \neq 0$ at point $x = x_j^1$. The curve $C_j(x)$ is monotonically decreasing for $x < x_j$ because if it were increasing for $x < x_j$, the intersection would not have happened in the first place. Thus, for $x < x_j$, $\min_m C_m(x) = C_j(x) < C_0(x_j)$. Thus, $\min_m C_m$ achieves its maximum at the point x_j and $x^* = x_j = \max_i x^{(i)}$, $1 \leq i, j \leq M - 1$. It follows that the (maximized) minimum capacity at the optimal point x^* is $C_0(x^*)$ or $C_j(x^*)$.

b) *Special Case:* If $C_0 = \min_i C_i$ at $x = x_0$, then no intersection of C_0 will take place with any curve C_j , $j = 1, \dots, M - 1$ for any $x > x_0$. In this case, the optimal UAV location is $x^* = x_0$.

¹It is possible that $C_0(x)$ may intersect more than one curve at the point x_j . However, this does not affect the final result of our argument.

2) *Solution of Two-Dimensional Problem:* The one-dimensional optimization problem can be extended in a straightforward manner to the two-dimensional setting. In this regard, we define the distance D_i as the Euclidean distance between the 0th and the i th sensors. Furthermore, let us define the vector \mathbf{d}_i as the (variable) vector that points from sensor 0 to sensor i . Let us define $d_i := \|\mathbf{d}_i\|_2$ where $0 < d_i \leq D_i$. Now, let the point of intersection between C_0 and C_i be given by

$$C_0(d_i) = C_i(D_i - d_i) \implies \frac{P_0}{z^2 + d_i^2} = \frac{P_i}{z^2 + (D_i - d_i)^2} \quad (29)$$

$$\implies (P_0 - P_i)d_i^2 - 2P_0D_id_i + P_0z^2 - P_iz^2 + P_0D_i^2 = 0, \quad (30)$$

$$\implies d_i^* = \frac{-b - \sqrt{b^2 - 4ac}}{2a}, \quad (31)$$

where $a := P_0 - P_i$, $b := -2P_0D_i$ and $c := P_0z^2 - P_iz^2 + P_0D_i^2$. The solution $\frac{-b + \sqrt{b^2 - 4ac}}{2a}$ is discarded since it is negative. Then, the two-dimensional point, where C_0 and C_i intersect, is

$$\begin{bmatrix} x^{(i)} \\ y^{(i)} \end{bmatrix} = \begin{bmatrix} x_0 \\ y_0 \end{bmatrix} + \begin{bmatrix} \delta x_i^* \\ \delta y_i^* \end{bmatrix}, \quad (32)$$

where $\delta x_i^* := d_i^* \cos(\theta_i)$ and $\delta y_i^* := d_i^* \sin(\theta_i)$ where θ_i is the angle that \mathbf{d}_i makes with x -axis. Here, the optimal solution (optimal location of the UAV) for the three dimensional max-min problem is $(x^{(j)}, y^{(j)})$ where $j = \arg \max_i \|\mathbf{x}^{(i)}\|_2$, and $\mathbf{x}^{(i)}$ is defined as $\mathbf{x}^{(i)} := [x^{(i)} \quad y^{(i)}]^T$.

3) *Optimization plots of (26):* Fig. 4 illustrates the maximum achievable rate (in nats/s/Hz) in the uplink channel between the m th sensor and the UAV, denoted as C_m , for five different sensors. This problem is formulated as a Max-min optimization problem. From the graph, C_0 curve—represented by orange color—intersects with other four curves at points $x^{(i)}$, where $i = 1, 2, 3, 4$. Among these intersections, the point $x^{(4)}$ notably produces the largest minimum value for C_m across all sensors. For Fig. 4, the parameter values are as follows: The total link distance $D = 1000$ m, the number of the sensors is $M = 5$, the location of sensors are $\mathbf{x}_m = [0, 200, 400, 700, 1000]$, the power transmitted by the sensors is $\mathbf{P}_m = [2.5, 3, 3.5, 4, 5]$ (left) and $\mathbf{P}_m = [0.3, 3, 3.5, 4, 5]$ (right), the factor $\beta_0 = 0.2$, the noise power $\sigma_0^2 = 1 \times 10^{-6}$ and the height of UAV $z = 300$ m.

As for the right graph in Fig. 4 represents to the special case previously discussed in III-B1b. Here, C_0 corresponds to $\min_m C_m$ for all $x > x_0$. Here, C_0 does not intersect with any of the four remaining curves. As a result, we find that the optimal point that maximizes $\min_m C_m$ coincides with x_0 .

IV. SOLAR ENERGY HARVESTING AND ENERGY CONSUMPTION MODELS OF HOVERING UAVS

A. Energy Harvesting Model

In this paper, we assume that the UAV is fitted with a large enough solar panel so that the energy required by the UAV rotors as well as laser transmission to the OGS is provided solely by sunlight. In this case, the atmospheric transmittance

at an altitude z in the region above the clouds is determined as [8]

$$\alpha_0(z) = A_0 - B_0 \exp\left(-\frac{z}{\delta}\right), \quad (33)$$

where A_0 is the maximum value of atmospheric transmittance, B_0 is the extinction coefficient of the atmosphere in m^{-1} , and δ is the scale height of the earth in m. Besides this, the presence of clouds and the dirt in air will further reduce the sunlight energy reaching the UAV. In this regard, let us define the energy attenuation through clouds and dirt as $\alpha_c(Z_c) := \exp(-\beta_c Z_c)$ and $\alpha_d(Z_d) := \exp(-\beta_d Z_d)$. The quantities β_c and β_d denote the extinction coefficient of the cloud and the air mediums, respectively. Then, the harvested solar power at the UAV, denoted by P_H , is given by [8]

$$P_H(z) = \begin{cases} \eta_p A G_r \alpha_0(z), & z > Z_c + Z_d, \\ \eta_p A G_r \alpha_0(z) \alpha_c(Z_c + Z_d - z), & Z_d < z < Z_c + Z_d, \\ \eta_p A G_r \alpha_0(z) \alpha_c(Z_c) \alpha_d(Z_d - z), & z < Z_d, \end{cases} \quad (34)$$

where η_p is the photoconversion efficiency of photovoltaic cells, A is the active surface area of the photovoltaic array in m^2 and G_r denotes the average solar radiation on earth in W/m^2 .

B. Energy Consumption Model

It has been shown in [1] that the power consumed by a UAV while hovering is

$$P_0 = \sqrt{\frac{(mg)^3}{2\pi r^2 \rho}}, \quad (35)$$

where m is the mass of the UAV and the solar panels in kg, g is the gravitational acceleration: $g := 9.8$ m/s, r is the radius of the propeller in meters, and ρ is the density of air at a given height and temperature in kg/m^3 . For instance, for a UAV with a total mass of 5 kg, propeller radius of 0.5 m and the air density $\rho = 1.225$ kg/m^3 , the power required to sustain the UAV in the hovering position is approximately 247 Watts. Thus, the height of the UAV (z) and the area of the solar panel, A , has to be such that the harvested power $P_H(z)$ has to be more than 247 Watts for this particular scenario.

With the advancements in photovoltaic technology, the power-to-weight and the power-to-area ratio of the solar arrays has improved considerably over the last decade. For instance, the flexible textile solar panels devised by SolarCloth System (France) can deliver power densities up to 170 W/m^2 with an average weight density of 500 g/m^2 [37]. This leads to an energy density of 340 W/kg with the textile solar panels. The United States based Ascent Solar Technologies developed super lightweight high-quality crystalline silicon solar arrays in 2016 that can deliver energy density up to 1700 W/kg . The highly flexible perovskite solar arrays have been shown to achieve a power density of 23 W/g [38]. These high power-to-weight and power-to-area ratio arrays are highly suitable for deployment on unmanned aerial vehicles, weather balloons and aeroplanes [38].

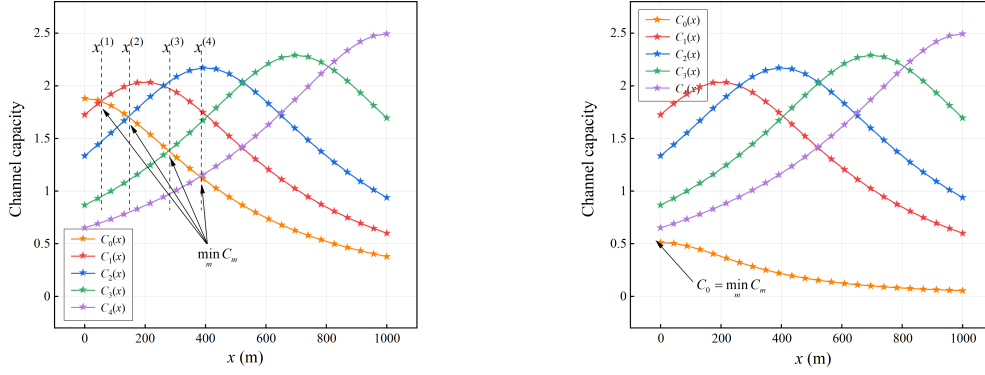


Fig. 4. This figure shows the Capacity Curves for Max-min fairness problem.

V. END-TO-END RATE OF THE SENSOR-UAV-OGS LINK FOR SOLAR UAV

As discussed before, the UAV assumes the role of a relay to connect the sensor field with the OGS: The sensor-to-UAV link is RF whereas the UAV-to-OGS link is optical wireless. In this section, we consider the end-to-end channel capacity for this hybrid RF/FSO link that utilizes a solar energy harvesting amplify-and-forward (AF) or decode-and-forward (DF) UAV relay. We denote the capacity in the laser backhaul (UAV-to-OGS link) by the symbol C_b .

A. AF Relay

Let X denote the sum signal reaching the AF relay from the sensor network. We have that

$$X = \underbrace{\sum_{m=0}^{M-1} \sqrt{\frac{P_m \beta_0}{z^2 + (x - x_m)^2 + (y - y_m)^2}}}_{S_X} + \underbrace{\sum_{m=0}^{M-1} N_m}_{N_X}, \quad (36)$$

where N_m are the i.i.d. Gaussian random variables: $N_m \sim \mathcal{N}(0, \sigma_0^2)$ where σ_0^2 is the thermal noise variance in a single sensor channel. Let σ_s^2 denote the total noise variance in the aggregate sensor channel. Then, $\sigma_s^2 = M\sigma_0^2$ where M is the total number of sensors. By definition, $N_X \sim \mathcal{N}(0, \sigma_s^2)$.

The laser signal retransmitted by the AF relay to the OGS is $Y = GX$, where G is the voltage amplification factor. Let us assume that the average harvested power is P_H Watts and the average power to sustain the UAV in the air is P_0 Watts. Then, the net power available for the purpose of signal transmission is $P_H - P_0$. Since the relay cannot transmit more than the net power, we have that

$$P_H - P_0 \geq \mathbb{E}[G^2 X^2] = G^2 \mathbb{E}[X^2] = G^2 \mathbb{E}[S_X^2 + N_X^2 + 2S_X N_X] = G^2 S_X^2 + G^2 \sigma_s^2 \quad (37)$$

$$\implies G^2 \leq \frac{P_H - P_0}{S_X^2 + \sigma_s^2} \implies G \leq \sqrt{\frac{P_H - P_0}{S_X^2 + \sigma_s^2}}. \quad (38)$$

Here, for the purpose of analysis, we set G equal to the maximum possible value it can attain: i.e., $G = \sqrt{\frac{P_H - P_0}{S_X^2 + \sigma_s^2}}$.

The received signal at the OGS is denoted by Z . We have that

$$Z = \eta \mathfrak{h} Y + N = \eta \mathfrak{h} G X + N = \eta \mathfrak{h} G (S_X + N_X) + N = \eta \mathfrak{h} G S_X + \eta \mathfrak{h} G N_X + N. \quad (39)$$

where \mathfrak{h} is the (random) optical channel gain in the backhaul, η is the photoconversion efficiency at the OGS receiver and N

is a Gaussian random variable which represents thermal noise at the OGS optical receiver: $N \sim \mathcal{N}(0, \sigma_N^2)$. The conditional end-to-end rate (in bits/seconds/Hz) for the AF relay is

$$\begin{aligned} C(h) &= \ln \left(1 + \frac{(\eta \mathfrak{h} G S_X)^2}{(\eta \mathfrak{h} G)^2 \sigma_s^2 + \sigma_N^2} \right) \\ &= \ln \left(1 + \frac{\eta^2 h^2 \left(\frac{P_H - P_0}{S_X^2 + \sigma_s^2} \right) S_X^2}{\eta^2 h^2 \left(\frac{P_H - P_0}{S_X^2 + \sigma_s^2} \right) \sigma_s^2 + \sigma_N^2} \right) \end{aligned} \quad (40)$$

Finally, the unconditional rate (averaged over \mathfrak{h}) is $C = \int_0^\infty C(h) f_{\mathfrak{h}}(h) dh$.

1) *Asymptotic Case 1:* When the SNR in the aggregate sensor-to-UAV channel is high, i.e., $S_X^2 \gg \sigma_s^2$ and the SNR in the UAV-to-OGS optical channel is low, i.e., $\sigma_N^2 \gg \eta^2 h^2 \left(\frac{P_H - P_0}{S_X^2 + \sigma_s^2} \right) \sigma_s^2$, then,

$$\begin{aligned} C(h) &= \ln \left(1 + \frac{\eta^2 h^2 \left(\frac{P_H - P_0}{S_X^2 + \sigma_s^2} \right) S_X^2}{\eta^2 h^2 \left(\frac{P_H - P_0}{S_X^2 + \sigma_s^2} \right) \sigma_s^2 + \sigma_N^2} \right) \\ &\approx \ln \left(1 + \frac{\eta^2 h^2 (P_H - P_0)}{\sigma_N^2} \right). \end{aligned} \quad (41)$$

In this scenario, we note that the backhaul channel dominates the end-to-end capacity. To understand the effect of link distance on the capacity, we note that for the fading scenario, the signal strength's dependence on link distance is only through pointing error² and not scintillation. Therefore, without loss of generality, we assume that the optical channel suffers fading mainly due to pointing error. Under this assumption, the composite channel gain is $\mathfrak{h} = \mathfrak{h}_p h_a h_c$ with PDF:

$$f_{\mathfrak{h}}(h) = \frac{\Phi}{h_a h_c} \left(\frac{h}{h_a h_c} \right)^{\frac{\theta^2 - \sigma^2}{\sigma^2}} \cdot \mathbb{1}_{[0, B h_a h_c]}(h).$$

In this case, the unconditional rate is

$$C \approx \int_0^{B h_a h_c} \ln \left(1 + \frac{\eta^2 h^2 (P_H - P_0)}{\sigma_N^2} \right) \cdot \frac{\Phi}{h_a h_c} \left(\frac{h}{h_a h_c} \right)^{\frac{\theta^2 - \sigma^2}{\sigma^2}} dh \quad (42)$$

Recall that from (4), $\Phi = \frac{\theta^2}{\sigma^2} \left(\frac{1}{B} \right)^{\frac{\theta^2}{\sigma^2}}$. To get a closed-form expression, we assume the common result that $\theta^2 \approx 2\sigma^2$, which is justified in [14]. Under this assumption, (42) can

²It is shown later in the same section that the loss in end-to-end capacity due to pointing error increases directly with link distance.

be further simplified as

$$\begin{aligned} C &\approx \int_0^{Bh_a h_c} \frac{2}{B^2 h_a^2 h_c^2} \cdot \ln \left(1 + \frac{\eta^2 (P_H - P_0) h^2}{\sigma_N^2} \right) \cdot h \, dh \\ &= \left(1 + \frac{\sigma_N^2}{\eta^2 h_a^2 h_c^2 (P_H - P_0) B^2} \right) \\ &\quad \cdot \ln \left(1 + \frac{\eta^2 h_a^2 h_c^2 B^2 (P_H - P_0)}{\sigma_N^2} \right) - 1 \end{aligned} \quad (43)$$

In the presence of fading due to pointing error, the relationship between link distance and attenuation due to pointing error is not clear. In this scenario, to show that the channel capacity of the laser link is maximized when the UAV lies as close as possible to the OGS, we first show that C is monotonically increasing in t where $t := \frac{\eta^2 h_a^2 h_c^2 B^2 (P_H - P_0)}{\sigma_N^2} > 0$. Then, $C(t) = (1 + \frac{1}{t}) \ln(1 + t) - 1$, and by taking the first derivative, we have that $C'(t) = \frac{t - \ln(1+t)}{t^2} > 0$, since $t > \ln(1 + t)$ for all $t > 0$. Thus, C is monotonically increasing in t . This implies that—for a fixed height z —we want to maximize only B, h_a and h_c to maximize C since the term $\frac{\eta^2 h_a^2 h_c^2 (P_H - P_0)}{\sigma_N^2}$ does not depend on UAV location in (x, y) plane. The quantities B, h_a and h_c are maximized only at $(0, 0, z)$, which is exactly on top of the OGS location on ground. In other words, for a fixed UAV height z , the optimal UAV position in the (x, y) plane is the same as the position of the OGS.

2) *Asymptotic Case 2:* When the SNR in the optical UAV-to-OGS channel is high compared to the aggregate sensor-to-UAV channel such that $\sigma_N^2 \ll \eta^2 h^2 \left(\frac{P_H - P_0}{S_X^2 + \sigma_s^2} \right) \sigma_s^2$, then the channel capacity is approximated as

$$\begin{aligned} C(h) &= \ln \left(1 + \frac{\eta^2 h^2 \left(\frac{P_H - P_0}{S_X^2 + \sigma_s^2} \right) S_X^2}{\eta^2 h^2 \left(\frac{P_H - P_0}{S_X^2 + \sigma_s^2} \right) \sigma_s^2 + \sigma_N^2} \right) \\ &\approx \ln \left(1 + \frac{\eta^2 h^2 \left(\frac{P_H - P_0}{S_X^2 + \sigma_s^2} \right) S_X^2}{\eta^2 h^2 \left(\frac{P_H - P_0}{S_X^2 + \sigma_s^2} \right) \sigma_s^2} \right) = \ln \left(1 + \frac{S_X^2}{\sigma_s^2} \right), \end{aligned} \quad (44)$$

which is simply the capacity of the aggregate sensor-to-UAV channel and its maximum value depends only on the positions and transmitted powers of the sensors (the optimum UAV position for this case was derived in Section III).

3) *Asymptotic Case 3:* For large noise power σ_N^2 at the OGS receiver such that, $\sigma_N^2 \gg \eta^2 h^2 \left(\frac{P_H - P_0}{S_X^2 + \sigma_s^2} \right) \sigma_s^2$, the approximate end-to-end capacity is

$$C(h) \approx \ln \left(1 + \frac{\eta^2 h^2 \left(\frac{P_H - P_0}{S_X^2 + \sigma_s^2} \right) S_X^2}{\sigma_N^2} \right). \quad (45)$$

In this asymptotic case, the value of σ_N^2 does not play any role in determining the optimal UAV position since the optimal position depends only on the numerator.

B. DF Relay

The conditional end-to-end rate for a DF relay scheme is given by

$$C(h, x, y, z) = \min(C_b(h, x, y, z), C_s(x, y, z)). \quad (46)$$

The dependence of aggregate sensor channel capacity C_s on UAV location (x, y, z) is evident through (12). The capacity in the backhaul, C_b , depends on the UAV location through the distribution of channel coefficient \mathbb{h}_p which is a function of (x, y, z) because of the factor B (as depicted in (5)). Additionally, C_b also depends on channel coefficients h_a and h_c —which are defined by (8) and (7), respectively—which also depend on the UAV position. The average end-to-end rate of the DF link is

$$\begin{aligned} C(x, y, z) &= \int_0^{Bh_a h_c} C(h, x, y, z) f_{\mathbb{h}}(h) \, dh \\ &= \int_0^{Bh_a h_c} \min \left(\ln \left(1 + \frac{((P_H - P_0)h\eta)^2}{\sigma_N^2} \right), \right. \\ &\quad \left. \sum_{m=0}^{M-1} \ln \left(1 + \frac{P_m \beta_0}{\sigma_0^2 [z^2 + (x - x_m)^2 + (y - y_m)^2]} \right) \right) f_{\mathbb{h}}(h) \, dh. \end{aligned} \quad (47)$$

We can obtain a closed-form expression for the approximate channel capacity when the pointing error is the major contributing factor to signal fading [14]. In that case, the approximate closed-form expression of capacity, denoted by \tilde{C} , is [14]

$$\begin{aligned} \tilde{C}(x, y, z) &= \Phi \frac{(P_H - P_0)^2 \eta^2}{\sigma_N^2} \frac{\sigma^2}{\theta^2 + 2\sigma^2} \left(\min(\hat{h}, h^*, Bh_a h_c) \right)^{\frac{\theta^2 + 2\sigma^2}{\sigma^2}} \\ &\quad + \Phi \sigma^2 \left(\frac{(\min(\hat{h}, h^*, Bh_a h_c) - \min(h^*, Bh_a h_c)) \alpha}{\theta^2} \right. \\ &\quad - \frac{(\min(\hat{h}, h^*, Bh_a h_c))^{\frac{2\sigma^2 + \alpha\theta^2}{\alpha\sigma^2}} \times \alpha \left(\frac{(P_H - P_0)\eta}{\sigma_N} \right)^{\frac{2}{\alpha}}}{\alpha\theta^2 + 2\sigma^2} \\ &\quad + \frac{(\min(h^*, Bh_a h_c))^{\frac{2\sigma^2 + \alpha\theta^2}{\alpha\sigma^2}} \times \alpha \left(\frac{(P_H - P_0)\eta}{\sigma_N} \right)^{\frac{2}{\alpha}}}{\alpha\theta^2 + 2\sigma^2} \\ &\quad - \frac{\min(\hat{h}, h^*, Bh_a h_c)^{\frac{2\sigma^2 + \alpha\theta^2 - 2\alpha\sigma^2}{2\sigma^2}} \times \left(\frac{(P_H - P_0)\eta}{\sigma_N} \right)^{\frac{2-2\alpha}{\alpha}}}{\alpha\theta^2 + 2\sigma^2 - 2\alpha\sigma^2} \\ &\quad \left. + \frac{\min(h^*, Bh_a h_c)^{\frac{2\sigma^2 + \alpha\theta^2 - 2\alpha\sigma^2}{2\sigma^2}} \times \left(\frac{(P_H - P_0)\eta}{\sigma_N} \right)^{\frac{2-2\alpha}{\alpha}}}{\alpha\theta^2 + 2\sigma^2 - 2\alpha\sigma^2} \right) \\ &\quad + \sum_{m=0}^{M-1} \ln \left(1 + \frac{P_m \beta_0}{\sigma_0^2 [z^2 + (x - x_m)^2 + (y - y_m)^2]} \right) \\ &\quad \times \frac{\Phi \sigma^2}{\theta^2} \left((Bh_a h_c)^{\frac{\theta^2}{\sigma^2}} - \left(\min(h^*, Bh_a h_c) \right)^{\frac{\theta^2}{\sigma^2}} \right), \end{aligned} \quad (48)$$

where $h^* := \frac{\sigma_N \sqrt{\prod_{m=0}^{M-1} \left(1 + \frac{P_m \beta_0}{\sigma_0^2 [z^2 + (x - x_m)^2 + (y - y_m)^2]} \right) - 1}}{(P_H - P_0)\eta}$, $\hat{h} := \frac{\sigma_N}{(P_H - P_0)\eta}$ and $\alpha \gg 1$.

1) *Asymptotic Case 1:* When the SNR in the aggregate sensor-to-UAV channel is high compared to the SNR in the optical backhaul UAV-to-OGS channel—that is σ_N^2 is large—the capacity in the backhaul C_b dominates the end-to-end rate. In this case, the average end-to-end rate is approximately

$$C(x, y, z) = \int_0^{Bh_a h_c} \ln \left(1 + \frac{((P_H - P_0)h\eta)^2}{\sigma_N^2} \right) f_{\mathbb{h}}(h) \, dh, \quad (49)$$

which is similar to the asymptotic case 1 for AF scheme in V-A1. Therefore, for this asymptotic case, the optimal UAV based DF relay position in the (x, y) plane is the same as the position of the OGS.

2) *Asymptotic Case 2*: When the SNR in the aggregate sensor-to-UAV channel is low compared to the SNR in the optical UAV-to-OGS channel—that is σ_N^2 is low—then the capacity in the aggregate sensor channel, C_s , is dominant. In this case, the average end-to-end rate in (47) can be simplified to

$$C(x, y, z) = \sum_{m=0}^{M-1} \ln \left(1 + \frac{P_m \beta_0}{\sigma_0^2 [z^2 + (x - x_m)^2 + (y - y_m)^2]} \right). \quad (50)$$

In other words, the optimal location of UAV depends only on the positions and transmitted powers of the sensors which is studied in detail in Section III.

VI. THREE-DIMENSIONAL POSITION OPTIMIZATION OF SOLAR UAV FOR SENSOR-UAV-OGS LINK

In our optimization analysis, our primary objective is to enhance the end-to-end capacity of the sensor-UAV-OGS link by optimizing the solar-powered UAV position in x, y and z dimensions. The motivation for optimization in (x, y) plane stems from the fact that the end-to-end rate of sensor-UAV-OGS link depends on both the sensor-to-UAV link and the UAV-to-OGS link: If the UAV is too close to the OGS, the sensor-to-UAV link will suffer performance degradation, and if the UAV is too close to the sensor field, the UAV-to-OGS link will underperform. Therefore, an optimal choice of (x, y) coordinates of the UAV is important to maintain an optimum end-to-end rate.

The height z of the UAV is important in that it decides the amount of energy harvested from the sun as well as the performance of sensor-to-UAV and UAV-to-OGS links. If the UAV is placed too high from the ground, the UAV will harvest more solar energy but it will lie further away from the sensors and the OGS which will minimize the end-to-end rate. On the other hand, if the UAV is too close to the ground, the minimized harvested energy will affect the UAV-to-OGS link. Thus, an optimal height z is necessary to guarantee a maximum end-to-end capacity performance. Additionally, recognizing the impact of weather conditions on UAV placement, this study also caters to the affect of clouds on the optimal altitude choice for the UAV.

In this section, we consider the three-dimensional position optimization of a solar-powered UAV relay. For the optimization problem, we have standardized the position of all sensors (in meters) as follows: $\mathbf{x}_m = [700, 800, 900, 1000, 1200, 1400, 1500, 1600, 1800, 2000]$ and $\mathbf{y}_m = [800, 900, 1000, 1200, 1300, 1500, 1600, 1700, 1900, 2000]$. The default parameter values of our optimization problems are enumerated in Table I. The UAV position optimization

Symbol	Parameter	Simulation Value
a_d	Radius of OGS receiver telescope (m)	0.5
θ	Angular beamwidth (radians)	1×10^{-2}
σ	Angular pointing error standard deviation (radians)	1×10^{-2}
D	Distance between OGS and farthest sensor (m)	1000, 2000
Z_c	Distance sunlight travels through the cloud (m)	500
Z_d	Distance sunlight travels through dirt medium (m)	500
P_m	Power transmitted by the m th sensor (Watts)	0.2–5
β_0	Channel power gain at the reference distance from the sensor	0.2, 0.4, 0.6
M	Total number of sensors	10
A_0	Maximum value of atmospheric transmittance	0.8978
B_0	Extinction coefficient of the atmosphere (m^{-1})	0.2804
δ	Scale height of the earth (m)	8000
G_r	Average solar radiation on earth (W/m^2)	1361
A	Active surface area of the photovoltaic array (m^2)	2
η_p	Photoconversion efficiency of photovoltaic cells	0.4
η	Photoconversion efficiency at the OGS receiver	0.4
ψ_a	Attenuation/extinction factor of laser signal through air	0.001
ψ_c	Attenuation/extinction factor of laser signal through cloud	0.001–0.01
β_c	Attenuation/extinction factor of sunlight through cloud	0.001–0.02
β_a	Attenuation/extinction factor of sunlight through air	0.5
P_0	Power consumed by hovering UAV (Watts)	100
σ_0^2	Noise power of sensor-to-UAV link (Watts)	1×10^{-6}
σ_N^2	Thermal noise power at the OGS optical receiver (Watts)	1×10^{-10}

TABLE I
TABLE OF SIMULATION PARAMETERS

problem is formulated as

$$\begin{aligned} & \underset{x, y, z}{\text{maximize}} && C \\ & \text{subject to} && i) 0 < x < D, \\ & && ii) 0 < y < D, \\ & && iii) z > z_0. \end{aligned} \quad (51)$$

We employ numerical optimization techniques to solve this optimization problem. Here, the set of sensor's transmission power (in Watts) is given by $\mathbf{P}_m = [0.2, 0.4, 0.6, 0.8, 1, 1.2, 1.4, 1.6, 1.8, 2]$. The constraint $z > z_0$ corresponds to the condition $P_H(z) - P_0 > 0$, where $P_H(z)$ is a function of the UAV's altitude.

We now discuss the effect of UAV position on the end-to-end capacity through graphical illustrations. For the purpose of clarity, we only consider 2-D plots (functions of only one variable) to convey our results more effectively.

Fig. 5 illustrates the maximization of capacity as a function of x when the values of y and z are fixed at their optimal values: $y = y^*$ and $z = z^*$. This figure presents the distribution profiles of the Exponentiated Weibull (EW) fading of the UAV-to-OGS optical channel for various default parameters and its impact on UAV positioning. On the left, we can see from the illustration that a smaller tail probability corresponds to more severe fading. The center graph illustrates the channel capacity of a UAV based AF relay. Evidently, under different levels of EW fading conditions, it is observed that the fading severity plays a pivotal role in determining the optimal UAV position. The right figure illustrates the relationship between channel capacity and the UAV's position for a DF relay. For both AF and DF relays, we observe that as the fading levels becomes more severe, the optimal UAV location shifts closer to OGS in order to minimize the effect of fading in the optical channel.

Fig. 6 illustrates the impact of cloud attenuation factor ψ_c and optical noise power σ_N^2 on the UAV optimal location x^* for AF (left figure) and DF (right figure) relays. For one, this figure suggests an inverse relationship between x^* and these channel parameters due to the obvious reason that as the optical channel gets more impaired, the UAV has to shift closer to the OGS to improve the laser link (thereby minimizing x^*).

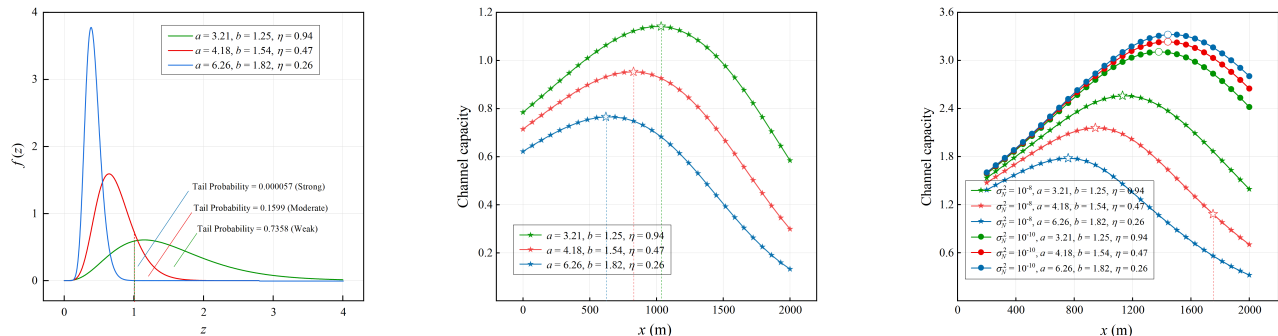


Fig. 5. The left figure shows Exponentiated Weibull fading with different parameters. The center and right figures shows capacity plots (as a function of x coordinate of UAV) for AF and DF relays, respectively.

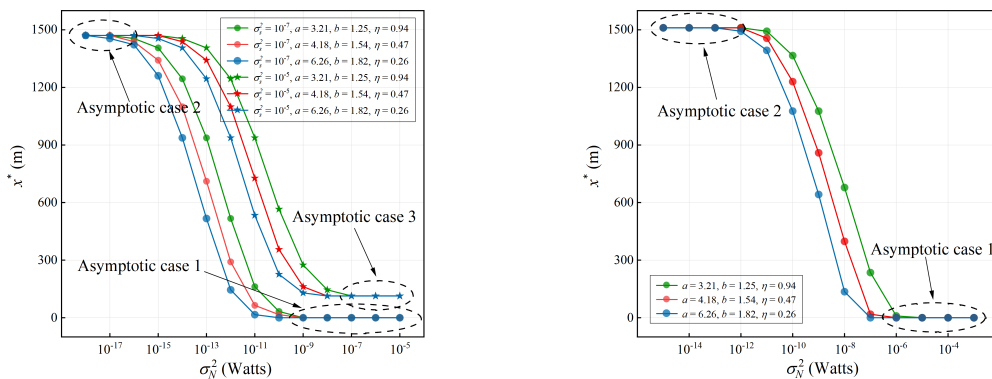


Fig. 6. This figure shows optimal location of UAV along x axis as a function of optical noise power σ_N^2 for AF scheme (left) and DF scheme (right) under Exponentiated Weibull fading. The attenuation factor $\psi_c = 0.003$.

This figure also highlights the asymptotic regimes of the two relays discussed in Section V-A and Section V-B. When the conditions for asymptotic case 1 are true for the AF relay (high SNR in sensor-to-UAV link and low SNR in UAV-to-OGS link), we note that the relay settles above the OGS, i.e., the relay optimal position $x^* \rightarrow 0$ as $\sigma_N^2 \rightarrow \infty$. On the other hand, for asymptotic case 3 (low SNR in both sensor-to-UAV and UAV-to-OGS links), the optimal position x^* becomes independent of noise power σ_N^2 as $\sigma_N^2 \rightarrow \infty$. Moreover, $\sigma_N^2 \rightarrow \infty \implies x^* \rightarrow \epsilon_0$ where $\epsilon_0 > 0$. This is in contrast with the DF relay case—shown in the right subfigure of Fig. 6—where the optimal position $x^* \rightarrow 0$ as $\sigma_N^2 \rightarrow 0$ irrespective of the SNR in the sensor-to-UAV link (asymptotic case 1 for DF relay). For high SNR in UAV-to-OGS link, the optimal UAV position is given by the solution to (III-A) for both AF and DF relays. In this case, the optimal solution depends only on the sensor locations and their transmitted powers.

Next, we investigate the impact of the UAV's altitude on the end-to-end capacity and explore how variations in the atmospheric environment affect the optimal altitude of the UAV. A critical consideration is that the energy $P_H(z)$ —harvested by solar panels on the UAV—depends on the altitude of the UAV and the solar energy attenuation coefficient due to atmospheric cloud layer, β_c . Consequently, when the UAV is positioned within the cloud layer, that is, where $Z_d < z < Z_c + Z_d$, we not only need to account for the attenuation of laser signal energy transmitted by the UAV through the cloud layer, but

also the attenuation of solar energy as it passes through the cloud layer before being absorbed by the UAV solar panels.

The interplay between the attenuation coefficients ψ_c and β_c —where ψ_c represents attenuation of laser signal through clouds and β_c denotes solar energy decay through clouds—is central to this optimization problem. It is crucial to emphasize that these parameters are inherently linked and are subject to simultaneous variations triggered by changing atmospheric conditions. However, these attenuation coefficients are strongly related to the wavelengths involved, and the wavelength-dependent attenuation is influenced by the cloud layer model which encompasses numerous variables. These include the size distribution of droplets within the cloud, the complex refractive indices related to the corresponding wavelengths as well as the shape of the particles [39]. The relationship between ψ_c and β_c , while crucial, is not the main focus of our study. Therefore, we have simplified the relationship between the two parameters into a linear model for our study in this paper.

Fig. 7 shows the end-to-end channel capacity as a function of the UAV altitude under the assumption $\beta_c = \psi_c$, modulated by various laser signal energy attenuation factors ψ_c . For this figure as well as the remaining figures in this paper, the sensor powers are distributed as $\mathbf{P}_m = [0.5, 1, 1.5, 2, 2.5, 3, 3.5, 4, 4.5, 5]$ Watts. Fig. 7 distinctly showcases the bimodal nature of the capacity curves as a function of altitude z . The critical point—where the slope changes instantly from negative to positive—occurs when the UAV is at the uppermost boundary of the cloud layer at

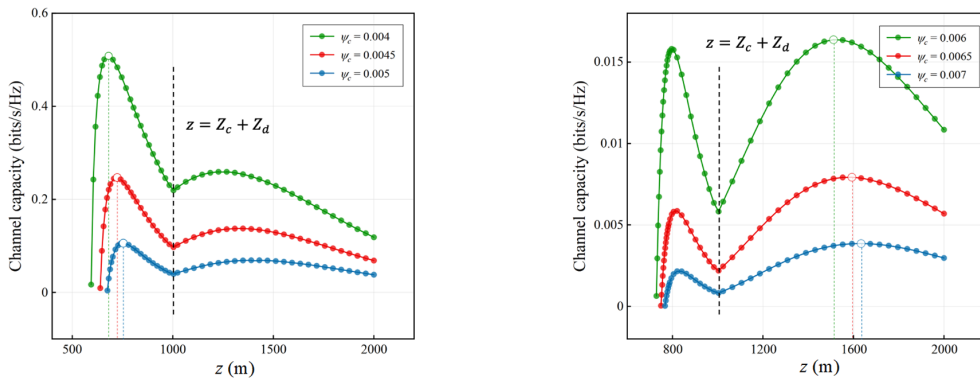


Fig. 7. The figure show the channel capacity as a function of UAV's altitude for different cloud attenuation factor ψ_c .

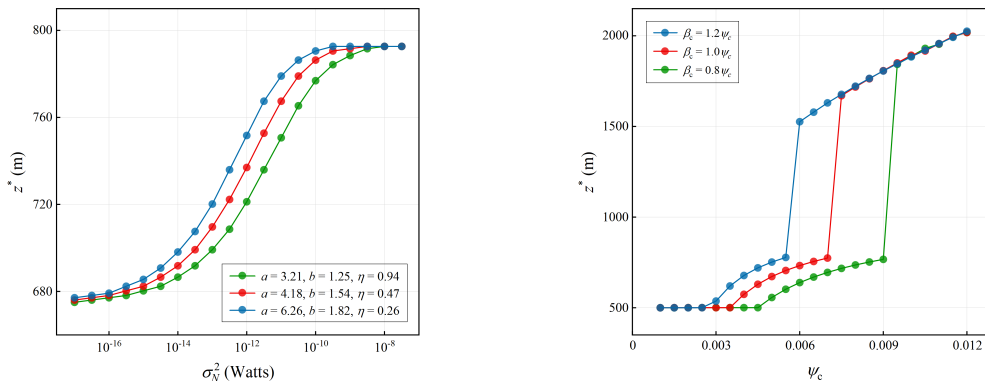


Fig. 8. The figures show the optimal height of UAVs as functions of σ_N^2 (left) and ψ_c (right) for different level fading channel (left) and different models of cloud attenuation factors (right).

$z = Z_c + Z_d = 1000$ m. A major insight from this figure is the increase in optimal UAV altitude as ψ_c escalates. This implies that in the adverse atmospheric conditions, the UAV tends to ascend closer to the sun to harvest more solar power to maintain the end-to-end link. A second major observation comes from the right subfigure in Fig. 7, where we note that as ψ_c exceeds a particular value, the optimal altitude shifts abruptly from the first peak (optimal height inside the cloud) to the second peak (optimal height outside the cloud). To provide a comprehensive understanding of the relationship between changes in the UAV optimal altitude and the atmospheric cloud conditions, a deeper investigation is essential.

In Fig. 8, the left curve depicts the relationship between the optimal altitude of the UAV and optical thermal noise power σ_N^2 . Here, we note that an increase in noise power—or conversely a decrease in the signal-to-noise ratio—prompts the UAV to fly higher to get closer to the sun in order to harvest more solar energy and reduce the impact of thermal noise on the performance. For large noise power, the optimal altitude becomes independent of the noise power due to (45). Moreover, $\sigma_N^2 \rightarrow 0 \implies z^* \rightarrow 0$ due to (44) and (36).

The right graph of Fig. 8 elucidates the impact of cloud channel coefficients ψ_c and β_c on the optimal height of UAV assuming a linear model between the two atmospheric parameters. We note that at minimal values of β_c and ψ_c , the optimal altitude for UAV converges at the bottom of the cloud $z = Z_d$, a fact that is attributed to minimal solar

energy attenuation by the clouds. However, below this altitude, the extinction coefficient of air—denoted as $\beta_a = 0.05$ —significantly diminishes solar energy, making the cloud base an equilibrium point for UAV positioning. As β_c and ψ_c increase due to formation of clouds, the UAV's optimal altitude starts to rise gradually. A particularly notable observation is that for each assumed linear model, there is an abrupt transition in the UAV's optimal height from within the cloud layer to the region above the top boundary of the cloud as ψ_c increases. This transition correlates with the dual peaks observed in Fig. 7, where the optimal height shifts from the location of the first peak to the second in an abrupt fashion. Finally, as ψ_c exceeds a certain threshold and continues to increase, the UAV's optimal altitude follows an approximately linear trajectory, with the three curves converging. This convergence is due to the fact that above the clouds, solar energy reaches the UAVs' solar panels without attenuation by the cloud, prompting the UAV to adopt similar altitude strategy across different atmospheric models.

VII. CONCLUSIONS

In this paper, we present a comprehensive model for a solar-powered UAV-assisted RF/FSO link that is aimed at facilitating data relay between distant sensors and an optical ground station (OGS). We demonstrate that there exists an optimal UAV position in three dimensions at which the end-to-end capacity is maximized. Our analysis also highlights

the impact of atmospheric conditions, such as cloud coverage, signal fading due to atmospheric turbulence and pointing error on the optical UAV-to-OGS link. A major finding of our study indicates that as the cloud channel becomes worse, the solar-powered UAV must be placed higher up in the sky to maximize the end-to-end rate. We believe that these findings will offer valuable insights for the design and implementation of future solar UAV-assisted RF/FSO communication links.

REFERENCES

- [1] H. V. Abeywickrama, B. A. Jayawickrama, Y. He, and E. Dutkiewicz, "Comprehensive Energy Consumption Model for Unmanned Aerial Vehicles, Based on Empirical Studies of Battery Performance," *IEEE Access*, vol. 6, pp. 58 383–58 394, 2018.
- [2] Y. Zeng, R. Zhang, and T. J. Lim, "Throughput Maximization for UAV-Enabled Mobile Relaying Systems," *IEEE Transactions on Communications*, vol. 64, no. 12, pp. 4983–4996, 2016.
- [3] J. Lyu, Y. Zeng, R. Zhang, and T. J. Lim, "Placement optimization of UAV-mounted mobile base stations," *IEEE Communications Letters*, vol. 21, no. 3, pp. 604–607, 2016.
- [4] Y. Qin, M. A. Kishk, and M.-S. Alouini, "On the Uplink SINR Meta Distribution of UAV-Assisted Wireless Networks," *IEEE Wireless Communications Letters*, vol. 12, no. 4, pp. 684–688, 2023.
- [5] —, "On the Downlink SINR Meta Distribution of UAV-assisted Wireless Networks," 2023.
- [6] Y. Zeng and R. Zhang, "Energy-efficient UAV communication with trajectory optimization," *IEEE Transactions on wireless communications*, vol. 16, no. 6, pp. 3747–3760, 2017.
- [7] M. Mozaffari, W. Saad, M. Bennis, and M. Debbah, "Efficient Deployment of Multiple Unmanned Aerial Vehicles for Optimal Wireless Coverage," *IEEE Communications Letters*, vol. 20, no. 8, pp. 1647–1650, 2016.
- [8] Y. Sun, D. Xu, D. W. K. Ng, L. Dai, and R. Schober, "Optimal 3D-trajectory design and resource allocation for solar-powered UAV communication systems," *IEEE Transactions on Communications*, vol. 67, no. 6, pp. 4281–4298, 2019.
- [9] S. Kandeepan, K. Gomez, L. Reynaud, and T. Rasheed, "Aerial-terrestrial communications: terrestrial cooperation and energy-efficient transmissions to aerial base stations," *IEEE Transactions on Aerospace and Electronic Systems*, vol. 50, no. 4, pp. 2715–2735, 2014.
- [10] K. Li, W. Ni, X. Wang, R. P. Liu, S. S. Kanhere, and S. Jha, "Energy-Efficient Cooperative Relaying for Unmanned Aerial Vehicles," *IEEE Transactions on Mobile Computing*, vol. 15, no. 6, pp. 1377–1386, 2016.
- [11] Y. Chu, C. Ho, Y. Lee, and B. Li, "Development of a Solar-Powered Unmanned Aerial Vehicle for Extended Flight Endurance," *Drones*, vol. 5, no. 2, 2021. [Online]. Available: <https://www.mdpi.com/2504-446X/5/2/44>
- [12] P. D. Diamantoulakis, K. N. Pappi, Z. Ma, X. Lei, P. C. Sofotasios, and G. K. Karagiannidis, "Airborne Radio Access Networks with Simultaneous Lightwave Information and Power Transfer (SLIPT)," in *2018 IEEE Global Communications Conference (GLOBECOM)*, 2018, pp. 1–6.
- [13] P. D. Diamantoulakis, G. K. Karagiannidis, and Z. Ding, "Simultaneous Lightwave Information and Power Transfer (SLIPT)," *IEEE Transactions on Green Communications and Networking*, vol. 2, no. 3, pp. 764–773, 2018.
- [14] M. S. Bashir and M.-S. Alouini, "Energy Optimization of a Laser-Powered Hovering-UAV Relay in Optical Wireless Backhaul," *IEEE Transactions on Wireless Communications*, vol. 22, no. 5, pp. 3216–3230, 2023.
- [15] P. Oettershagen, A. Melzer, T. Mantel, K. Rudin, T. Stastny, B. Wawrzacz, T. Hinzmann, K. Alexis, and R. Siegwart, "Perpetual flight with a small solar-powered UAV: Flight results, performance analysis and model validation," in *2016 IEEE Aerospace Conference*, 2016, pp. 1–8.
- [16] S. Morton, R. D'Sa, and N. Papanikolopoulos, "Solar powered UAV: Design and experiments," in *2015 IEEE/RSJ International Conference on Intelligent Robots and Systems (IROS)*, 2015, pp. 2460–2466.
- [17] Y. Fu, H. Mei, K. Wang, and K. Yang, "Joint Optimization of 3D Trajectory and Scheduling for Solar-Powered UAV Systems," *IEEE Transactions on Vehicular Technology*, vol. 70, no. 4, pp. 3972–3977, 2021.
- [18] R. I. Bor-Yaliniz, A. El-Keyi, and H. Yanikomeroglu, "Efficient 3-D placement of an aerial base station in next generation cellular networks," in *2016 IEEE international conference on communications (ICC)*. IEEE, 2016, pp. 1–5.
- [19] J.-H. Lee, K.-H. Park, Y.-C. Ko, and M.-S. Alouini, "Throughput Maximization of Mixed FSO/RF UAV-Aided Mobile Relaying With a Buffer," *IEEE Transactions on Wireless Communications*, vol. 20, no. 1, pp. 683–694, 2021.
- [20] R. Fan, J. Cui, S. Jin, K. Yang, and J. An, "Optimal node placement and resource allocation for UAV relaying network," *IEEE Communications Letters*, vol. 22, no. 4, pp. 808–811, 2018.
- [21] Z. Yang, C. Pan, M. Shikh-Bahaei, W. Xu, M. Chen, M. Elkashlan, and A. Nallanathan, "Joint altitude, beamwidth, location, and bandwidth optimization for UAV-enabled communications," *IEEE Communications Letters*, vol. 22, no. 8, pp. 1716–1719, 2018.
- [22] H.-T. Ye, X. Kang, J. Joung, and Y.-C. Liang, "Optimization for Wireless-Powered IoT Networks Enabled by an Energy-Limited UAV Under Practical Energy Consumption Model," *IEEE Wireless Communications Letters*, vol. 10, no. 3, pp. 567–571, 2021.
- [23] Q. Wu, Y. Zeng, and R. Zhang, "Joint trajectory and communication design for multi-UAV enabled wireless networks," *IEEE Transactions on Wireless Communications*, vol. 17, no. 3, pp. 2109–2121, 2018.
- [24] G. Vallero and M. Meo, "Modelling Solar Powered UAV-BS for 5G and Beyond," in *2021 19th Mediterranean Communication and Computer Networking Conference (MedComNet)*, 2021, pp. 1–8.
- [25] J.-S. Lee and K.-H. Yu, "Optimal Path Planning of Solar-Powered UAV Using Gravitational Potential Energy," *IEEE Transactions on Aerospace and Electronic Systems*, vol. 53, no. 3, pp. 1442–1451, 2017.
- [26] X. Zhang, V. A. Öberg, J. Du, J. Liu, and E. M. J. Johansson, "Extremely lightweight and ultra-flexible infrared light-converting quantum dot solar cells with high power-per-weight output using a solution-processed bending durable silver nanowire-based electrode," *Energy Environ. Sci.*, vol. 11, pp. 354–364, 2018. [Online]. Available: <http://dx.doi.org/10.1039/C7EE02772A>
- [27] Solar-electric 6-seat transporter, url = <https://www.solar-flight.com/solar-6-seat-transporter/>.
- [28] J. A. Duffie and W. A. Beckman, *Solar engineering of thermal processes*. John Wiley & Sons, 2013.
- [29] R. Dai, U. Lee, S. Hosseini, and M. Mesbahi, "Optimal path planning for solar-powered UAVs based on unit quaternions," in *2012 IEEE 51st IEEE Conference on Decision and Control (CDC)*. IEEE, 2012, pp. 3104–3109.
- [30] R. I. Bor-Yaliniz, A. El-Keyi, and H. Yanikomeroglu, "Efficient 3-D Placement of an Aerial Base Station in Next Generation Cellular Networks," in *2016 IEEE International Conference on Communications (ICC)*, 2016, pp. 1–5.
- [31] L. Zhang, A. Celik, S. Dang, and B. Shihada, "Energy-Efficient Trajectory Optimization for UAV-Assisted IoT Networks," *IEEE Transactions on Mobile Computing*, pp. 1–1, 2021.
- [32] X. Song, Z. Chang, X. Guo, P. Wu, and T. Hämmäläinen, "Energy Efficient Optimization for Solar-Powered UAV Communications System," in *2021 IEEE International Conference on Communications Workshops (ICC Workshops)*, 2021, pp. 1–6.
- [33] J. Marriott, B. Tezel, Z. Liu, and N. E. Stier-Moses, "Trajectory Optimization of Solar-Powered High-Altitude Long Endurance Aircraft," in *2020 6th International Conference on Control, Automation and Robotics (ICCAR)*, 2020, pp. 473–481.
- [34] X. Wang, Y. Yang, D. Wu, Z. Zhang, and X. Ma, "Mission-Oriented 3D Path Planning for High-Altitude Long-Endurance Solar-Powered UAVs With Optimal Energy Management," *IEEE Access*, vol. 8, pp. 227 629–227 641, 2020.
- [35] M. S. Bashir and M.-S. Alouini, "Optimal positioning of hovering UAV relays for mitigation of pointing error in free-space optical communications," *IEEE Transactions on Communications*, vol. 70, no. 11, pp. 7477–7490, 2022.
- [36] R. Barrios and F. Dios, "Exponentiated Weibull distribution family under aperture averaging for Gaussian beam waves," *Opt. Express*, vol. 20, no. 12, pp. 13 055–13 064, Jun 2012. [Online]. Available: <http://www.opticsexpress.org/abstract.cfm?URI=oe-20-12-13055>
- [37] "Special Edition / Textile Solar Panels for an Optimal Power-to-Weight Ratio," <https://www.boatsnews.com/story/32249/textile-solar-panels-for-an-optimal-power-to-weight-ratio>, accessed: 09-15-2022.
- [38] M. Kaltenbrunner et al., "Flexible high power-per-weight perovskite solar cells with chromium oxide–metal contacts for improved stability in air," *Nature Mater.*, vol. 14, p. 1032–1039, 2015.
- [39] F. Moll and M. Knappek, "Wavelength selection criteria and link availability due to cloud coverage statistics and attenuation affecting satellite, aerial, and downlink scenarios," in *Free-Space Laser Communications VII*, vol. 6709. SPIE, 2007, pp. 347–358.